



Fetal *indusium griseum* is a possible biomarker of the regularity of brain midline development in 3T MR imaging: A retrospective observational study

Ivana Pogledic¹  | Mihaela Bobić-Rasonja^{2,3} | Christian Mitter^{1,4} | Andrija Štajduhar^{3,5} | Ernst Schwartz⁶ | Marija Milković-Periša⁷ | Pascal A. Baltzer¹ | Maarten Lequin⁸ | Elisabeth Krampfl-Bettelheim⁹ | Gregor Kasprian¹ | Miloš Judaš³ | Daniela Prayer¹ | Natasa Jovanov-Milosevic^{2,3} 

¹Division of Neuroradiology and Musculoskeletal Radiology, Department of Biomedical Imaging and Image-guided Therapy, Allgemeines Krankenhaus, Medical University of Vienna, Vienna, Austria

²Department of Biology, School of Medicine, University of Zagreb, Zagreb, Croatia

³Croatian Institute for Brain Research, Scientific Center of Excellence for Basic, Clinical and Translational Neuroscience, School of Medicine University of Zagreb, Zagreb, Croatia

⁴Department of Systematic Anatomy, Center for Anatomy and Cell Biology, Medical University of Vienna, Vienna, Austria

⁵School of Medicine, School of Public Health "Andrija Štampar" University of Zagreb, Zagreb, Croatia

⁶Computational Imaging Research Lab, Department of Biomedical Imaging and Image-Guided Therapy, Medical University of Vienna, Vienna, Austria

⁷Department of Pathology and Cytology, School of Medicine, University Hospital Center Zagreb, University of Zagreb, Zagreb, Croatia

⁸Department of Radiology, University Medical Center Utrecht, Utrecht, The Netherlands

⁹Department of Obstetrics and Feto-maternal Medicine, Medical University of Vienna, Vienna, Austria

Correspondence

Natasa Jovanov-Milosevic, University of Zagreb School of Medicine, Šalata 12, Zagreb, Croatia.

Email: njovanov@mef.hr;

njovanov@hiim.hr

Funding information

Austrian Science Fund (FWF), Grant/Award Number: FWF grant: I 3925-B27; Medicinski Fakultet, Sveučilište u Zagrebu, Grant/Award Number: 10106-22-3116, 10106-23-2487 and BM0054; Hrvatska Zaklada za Znanost, Grant/Award Number: IP-2019-04-3182; European Regional Development Fund, Grant/Award Number: GA KK01.1.1.01.0007

Abstract

Introduction: This study aimed to assess the visibility of the *indusium griseum* (IG) in magnetic resonance (MR) scans of the human fetal brain and to evaluate its reliability as an imaging biomarker of the normality of brain midline development.

Material and methods: The retrospective observational study encompassed T2-w 3T MR images from 90 post-mortem fetal brains and immunohistochemical sections from 41 fetal brains (16–40 gestational weeks) without cerebral pathology. Three raters independently inspected and evaluated the visibility of IG in post-mortem and in vivo MR scans. Weighted kappa statistics and regression analysis were used to determine inter- and intra-rater agreement and the type and strength of the association of IG visibility with gestational age.

Results: The visibility of the IG was the highest between the 25 and 30 gestational week period, with a very good inter-rater variability (kappa 0.623–0.709) and excellent intra-rater variability (kappa 0.81–0.93). The immunochemical analysis of the

Abbreviations: CC, corpus callosum; GW, gestational weeks; IG, indusium griseum; MRI, magnetic resonance imaging; pm, post-mortem.

This is an open access article under the terms of the [Creative Commons Attribution-NonCommercial-NoDerivs](https://creativecommons.org/licenses/by-nc-nd/4.0/) License, which permits use and distribution in any medium, provided the original work is properly cited, the use is non-commercial and no modifications or adaptations are made.

© 2024 The Authors. *Acta Obstetrica et Gynecologica Scandinavica* published by John Wiley & Sons Ltd on behalf of Nordic Federation of Societies of Obstetrics and Gynecology (NFOG).

histoarchitecture of IG discloses the expression of highly hydrated extracellular molecules in IG as the substrate of higher signal intensity and best visibility of IG during the mid-fetal period.

Conclusions: The knowledge of developmental brain histology and fetal age allows us to predict the IG-visibility in magnetic resonance imaging (MRI) and use it as a biomarker to evaluate the morphogenesis of the brain midline. As a biomarker, IG is significant for post-mortem pathological examination by MRI. Therefore, in the clinical in vivo imaging examination, IG should be anticipated when an assessment of the brain midline structures is needed in mid-gestation, including corpus callosum thickness measurements.

KEYWORDS

corpus callosum, extracellular matrix, indusium griseum, malformations of cortical development, prenatal diagnosis, subplate, ultrasound

1 | INTRODUCTION

The *indusium griseum* (IG) is a paired cortical area situated paramedially on the trunk of corpus callosum (CC), confined with medial and lateral longitudinal Lancisi's stria, that continues anteriorly into the paraterminal gyrus, laterally into the cingulate cortex, and posteriorly into hippocampi in both hemispheres.¹ While the histoarchitectonics, neurochemistry, projections organization, and developmental features of the IG in humans have been studied in several studies,^{2,3} the animals' (mainly rodents) IG has been researched extensively.⁴⁻¹⁰ Although earliest descriptive studies claimed that human IG is rudimental,^{11,12} some studies of rodents' IG state that it is simply a supra-commissural continuation of the dentate gyrus,⁵⁻¹³ the recent studies in humans³ and rodents,¹⁴ as well as studies of patients who have Alzheimer's disease, suggest the contrary.¹⁵ They demonstrated that the development and maturation of human IG continue until the postnatal period,³ that differentiate into a distinct cortical subfield, and during the lifespan ages, and degenerate without significant reduction of its volume and pathological features specific to dentate gyrus aging.¹⁴

The fetal IG in humans has a transient lamination pattern that differs from the developmental patterns of limbic areas with the common ontogenic origin. A recent study¹⁶ suggests that IG might be a target of psychoactive drugs in the prenatal period, concurrently playing a significant role in the morphogenesis of the telencephalon midline, especially CC.¹⁷⁻²¹ The development and morphology of CC and IG can be abnormal in patients who suffer from neurodevelopmental disabilities and genetic disorders.²² The role of IG in the telencephalon midline morphogenesis in health and diseases, and the relative lack of data in that respect, has aroused scientific interest in IG. In particular, we were interested in the fetal human IG and the substrate of IG visibility in the post-mortem 3T T2-magnetic resonance imaging (MRI) found in our previous work.³

Key message

Indusium griseum (IG), visible on T2-weighted post-mortem MRI during mid-gestation due to the highly hydrated extracellular matrix, may influence the measurements of fetal corpus callosum thickness. Advanced imaging modalities improve IG visibility and strengthen IG as a fetal brain imaging biomarker.

There have only been a few studies concerning the visibility of IG in MR images in mature human brains.^{12,23,24} Within this retrospective observational study, we aimed to assess the validity of the IG visibility on post-mortem MR (pmMR) imaging (3T, T2) and in vivo MRI throughout the fetal development and the potential role of IG in the evaluation of the normality of prenatal brain development.

2 | MATERIAL AND METHODS

2.1 | MRI study population

The pmMR examinations of 90 fetuses staged between 16+4 and 39+5 gestational weeks (GW) (equal to weeks of amenorrhea) were retrospectively reviewed. The exclusion criteria were: (1) absent MRI, ultrasound, autopsy, or histological examination reports of fetal pathology, (2) insufficient image quality due to fetal autolytic changes, and (3) post-mortem interval to imaging longer than 36 h. In total, 19 cases with normal developmental parameters were selected for further analysis. To reveal whether the IG is observable on in vivo 3.0T MRI, 51 norm-typical cases without cerebral pathology and significant motion artifacts, ages 18+4 and 36+1 GW, were

inspected. A total of 24 cases with satisfactory super-resolution 3T in vivo images were included in the study.

2.2 | MRI methods

The three Tesla (3T) scanner (Magnetom Trio, Siemens Medical Solutions, Erlangen, Germany) with an ankle and knee coil, using a T2w-TSE sequence (TR 3180; TE_{eff} 137, FOV 144, base resolution 448, gap 0, flip angle 149°, duration 14:30min) was used for image acquisition. In addition, coronal scans of the fetal brain corresponding to plate 5 in the Bayer-Altman atlas were examined.²⁵

The in vivo 3T MR imaging was performed using Achieva, Philips Medical Systems, a five-element cardiac surface coil wrapped around the mother's abdomen without any sedation. The T2-weighted SSFSE (single-shot fast spin echo) sequences in three planes were analyzed (TR "shortest", TE 200ms, FOV 250×250, in-plane resolution 0.7×0.7 mm, slice thickness 3 mm). Specific absorption rates were kept under 2W/kg. In each case, a minimum of three as-orthogonal-as-possible acquisitions covering the fetal head in axial, coronal, and sagittal orientation were acquired. Each view was first denoised and upsampled, and all views of a case were consecutively combined by iterative motion correction and super-resolution reconstruction²⁶ to yield a single high-resolution isotropic volume with an isotropic voxel resolution of 0.5 mm.³

2.3 | Histological and immunohistochemical methods

Archive samples of 41 post-mortem human fetal brains, stage 14 to 40 GW, considered normal-typic based on clinical and histopathological assessment, were included in the histological study.

The entire brains were fixed by immersion in 4% formaldehyde in 0.1M phosphate buffer saline (PBS, pH=7.4) and cut to tissue blocks, further embedded in paraffin, subsequently cut in the coronal plane to 20µm thick sections and stained by Nissl and modified Mowry method.^{27,28} Adjacent tissue sections were immunohistochemically labeled as described previously^{18,21} for the primary antibodies: (1) rabbit anti-neuronal nuclear antigen, NEUN (AB104225, Abcam, Cambridge, UK); (2) rabbit anti-glial fibrillary acidic protein, GFAP (Z0334, Dako, Glostrup, Denmark); (3) mouse anti-chondroitin sulfate, CS-56 (C8035, Sigma, St. Louis, MO, USA); (4) rabbit anti-neurocan, NCAN (HPA036814, Sigma).

Olympus BX53 light microscope and images captured with the Olympus UC-90 digital camera (Olympus Corporation, Shinjuku, Tokyo, Japan) or a high-resolution digital slide scanner Nano-Zoomer 2.0RS (Hamamatsu, Japan) were used for analysis.

The fetal brains imaged post-mortem by MR were immersed in 10% formaldehyde solution (0.9% NaCl, 0.3% ZnSO₄·x7H₂O) for at least 2 weeks, embedded in paraffin, and cut to 4µm thick sections, stained with hematoxylin-eosin (HE) and scanned (Hamamatsu NanoZoomer 2.0-HT).

2.4 | Statistical analyses

Three experts independently rated the IG visibility on coronal T2-w scans without knowing the fetuses' gestational age. In this manuscript, and clinical articles and practices, the term gestational weeks (GW) refers to the period since the first day of the woman's last menstrual cycle, contrary to anatomical and developmental studies, where GW usually denotes the estimated period since conception. The score scale was from 0 to 5: 0 (not visible), 1 (uncertain visibility), 2 (poor visibility), 3 (satisfactory visibility), 4 (very good visibility), and 5 (excellent visibility). The rating was repeated after more than 6 months under the same conditions. Different regression models using linear, logarithmic, inverse, quadratic, and cubic fits investigated the association between visibility scores and fetal age. The R-square was used to indicate the variance of visibility explained by variations in GW and could range between 0 and 1. A *p*-value ≤0.05 was considered statistically significant. The interobserver agreement of the IG visibility was tested between two different raters and among all three raters by calculating weighted kappa statistics. Kappa (κ) values were interpreted as $\kappa < 0.20$ poor agreement, $\kappa = 0.21-0.40$ fair agreement, $\kappa = 0.41-0.60$ moderate agreement, $\kappa = 0.61-0.80$ good agreement, $\kappa = 0.81-1.00$ excellent agreement as in Landis and Koch.²⁹ Analyses were performed using SPSS Statistics 25 (IBM, US) and Medcalc 20.305 (Medcalc, Belgium) software.

3 | RESULTS

After critical inspection of 141 brains of fetuses, stages 16+4 to 39+5 GW, on pm 3T MR (T2-weighted) and on in vivo MR scans, the 19 without anomalies and with a post-mortem delay of less than 36 h were used for IG visibility rating while 24 for the analysis after super-resolution. The MR scans were correlated to the HE staining of the same brains and the matching (by age and anatomical position) histological sections stained for neuronal, glial, and extracellular matrix molecules from an additional 41 fetuses, which derived the following results.

3.1 | Molecular and histological correlates of the IG visibility

The IG can be distinguished on the coronal T2-w image as two small hyperintense spots situated paramedially above the CC, superimposed by a thin hypointense layer (Figure 1B,E). The sagittal plane of MRI most often is not ideally paramediosagittal and, therefore, can not scan precisely the entire anteroposterior axis of the IG zones in one section but fragment (Figure 2). Secondly, the assessment of IG visibility in the sagittal plane is challenging due to the size of the IG in the sagittal planes³ and the fact that the T2 hyperintense signal of the superpositioned space of the medial cerebral fissure interferes with the hyperintense signal of the ECM-enriched IG (Figure 2), while the hypointense signal of the IG cortical plate interferes with the cortical plate of the cingulate gyrus and the anterior cerebral

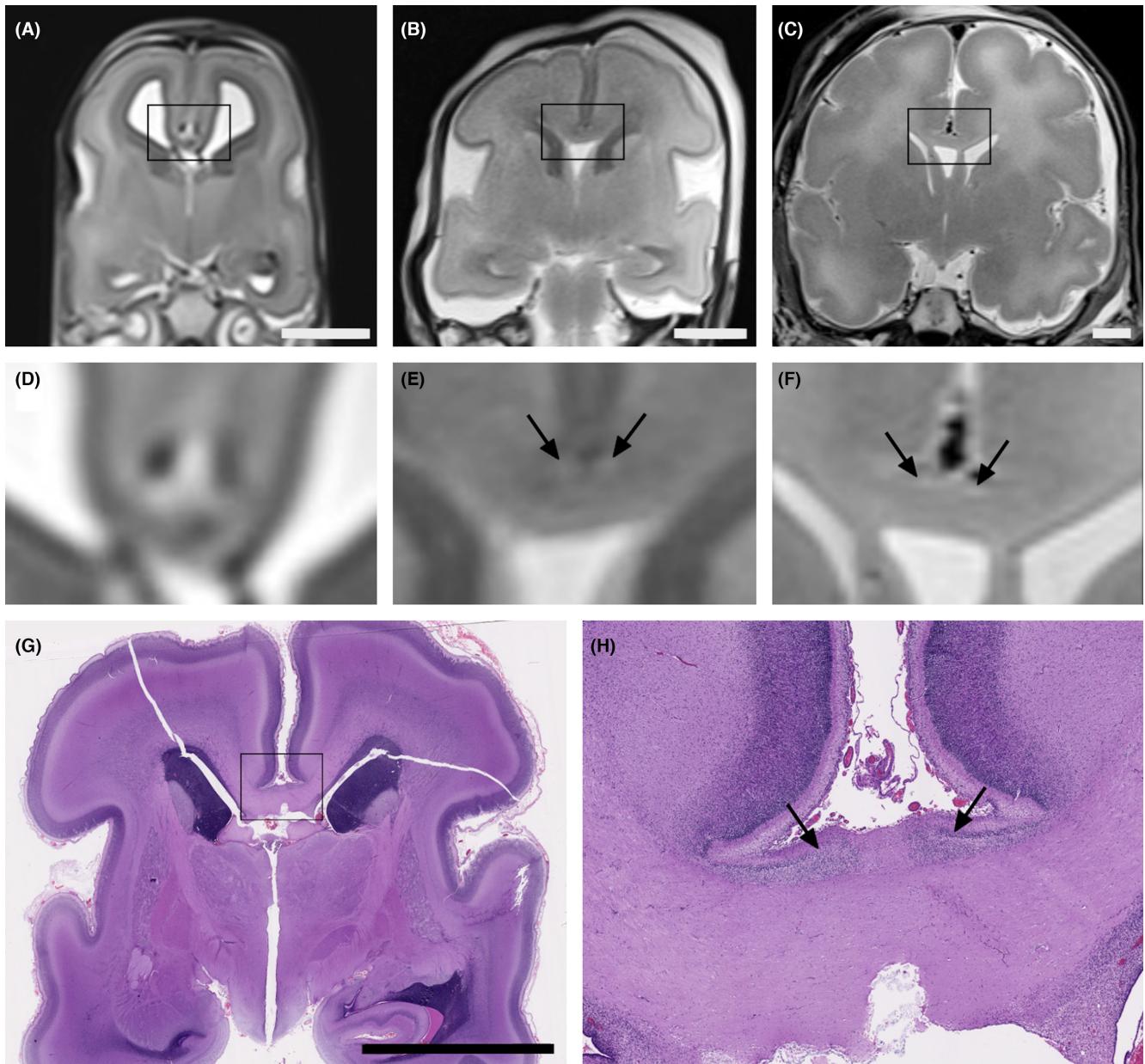


FIGURE 1 The panel represents post-mortem in situ MR (T2-w sequence, coronal plane) scans of the human brains obtained at three fetal stages showing different IG visibility and scans of the corresponding histological sections of the brain (presented in B and E) stained with hematoxylin-eosin (HE). A scan of a fetal brain at 16 GW (A) with the magnification of the cortical midline in (D) indicates the impossibility of IG visualization at this early developmental stage. Scan of a fetal brain at 21+2 GW is shown in (B); the enlarged view of the cortical midline reveals (arrows, E) the T2-w IG hyperintensity, and the corresponding histological section (G, H), stained by HE, reveals the histoarchitectonic structure of the IG. T2-w MR scan of the fetal brain in the coronal plane (C) shows weak IG visibility (arrows in F) at 39GW. Scale bars in all images mark 10mm. The MR images are not post-scanning processed.

artery (its pre- and supracallosal segment, [Figure 2](#)). In the coronal planes, these challenges are minimal, and the IG can be discerned with the highest chance at the level of the IG convexity around the genu and splenium of the corpus callosum. The magnetic resonance images in [Figures 1](#) and [2](#) are not post-scanning processed with a super-resolution pipeline or any other way but represent the scans used daily by radiologists and clinicians of relevant specialties.

The consequent histology of the same brain confirmed the IG developmental structure (coronal section, HE staining, see

[Figure 1G,H](#)). The histoarchitectonic and molecular correlates of IG visibility were distinguished by immunohistochemistry and are shown on the images of coronal sections of IG and ventromedial frontal lobe (cingulate gyrus) at the level of the frontal third of corpus callosum at the stage of 23rd GW ([Figure 3](#)). The IG emerges as a convexity dorsally on the trunk (body) of the CC and below the juxta-positioned limbus of the most ventral portion of the cingulate gyrus presented here by specific staining for histoarchitecture (Nissl, [Figure 3A](#)), neuronal (NEUN, [Figure 3B](#)), and glial (GFAP, [Figure 3C](#))

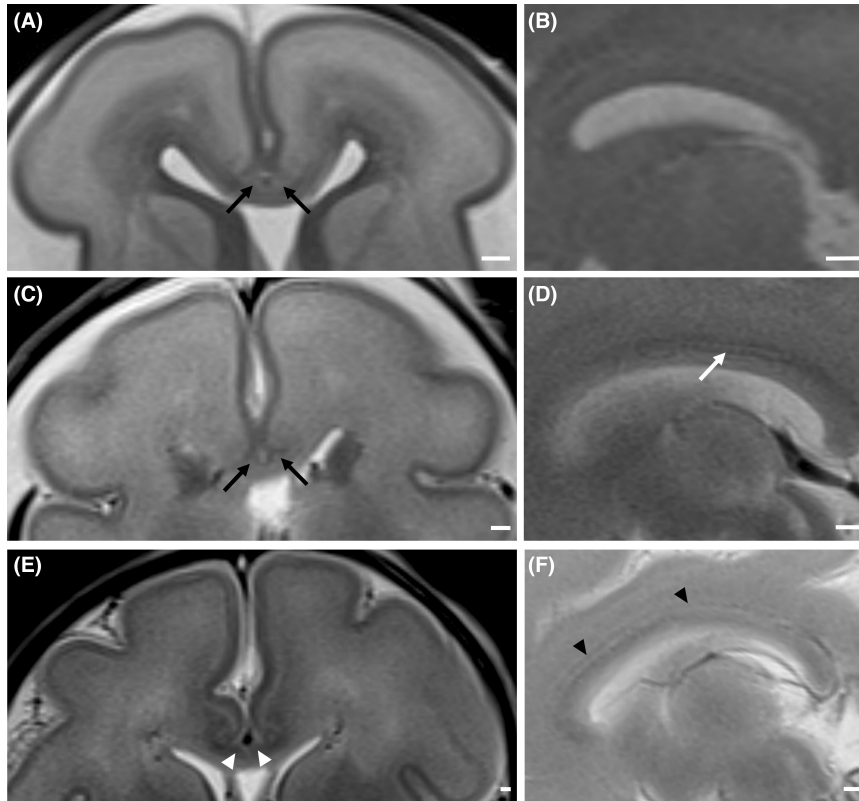


FIGURE 2 The panel presents representative in situ pmMR (T2-w sequence), coronal (A, C, E), and sagittal (B, D, F) plane scans of the human brains obtained at different fetal stages: 21+3 GW (A and B), 26+5 GW (C and D), and 30+1 GW (E and F), showing various visibility of IG. Black arrows (in A and C) indicate the higher signal intensity due to extracellular matrix (ECM) abundance in the transient fetal zone of the IG, while the white arrow (D) points to the IG cortical plate. The IG can be tracked only partially in the sagittal plane (B, D) since the MRI plane rarely passes through the entire sagittal axis of IG. At the beginning of the third trimester, the IG is visible as a small MRI hypointense area (white arrowheads in E) due to diminished ECM content. The anterior cerebral artery, its supracallosal segment, as a supra-callosally positioned hypointense line, is a confounding factor in the visualization of the IG in the sagittal planes and must not be misinterpreted as IG (black arrowheads in F). Scale bars in all images mark 2 mm. MRI images were not post-scanning processed.

elements. The chondroitin sulfate–proteoglycans (CS56, [Figure 3E](#)) and specifically neurocan (NCAN, [Figure 3F](#)) show an abundance of a hydrated matrix in the IG transient subplate zone (empty arrows in [Figure 3D–F](#)), which is the basis for hyperintense spots presented in MR images (open arrow in [Figure 1B,E](#)). The hypointense vertical stripes above the hyperintense areas in the MR images show the cortical plates of the future cingulate gyrus. Thus, the ECM-rich compartment corresponds to the T2 hyperintensity seen on MR scans. At the same time, the neuron-dense cortical plate, containing a minimum extracellular matrix, is a hypointense layer on MR scans ([Figure 1B,E](#)).

The brain midline's developmental structural and molecular pattern changes in the later fetal period. The differentiation of IG's cellular components advances at 33 GW, as shown by Nissl, NEUN, and GFAP staining ([Figure 4A–C](#)), flattening out the appearance on the coronal plane. The IG loses the developmental subplate zone and the abundance of hydrated extracellular molecules as evidenced by Mowry staining ([Figure 4D](#)), the chondroitin-sulfate proteoglycans (CS56, [Figure 4E](#)), and neurocan (NCAN, [Figure 4F](#)) immunolabeling. The CC-IG border (dashed line in [Figure 4](#)) is more challenging to discern at this stage. This histological organization corresponds

to the lower visibility of the IG in MR scans of fetal brains staged in the third trimester (see [Figure 1C,F](#)). The IG layers are more difficult to discern due to their reorganization, growth in the medial-lateral and frontal-occipital direction, neuronal dendrites arborization, axon elongation, and consequent cell-soma distancing in the mature stage.

3.2 | Association between IG MRI visibility and fetal developmental stage

The evaluation of MRI scans reveals that the visibility of the IG varies throughout fetal brain development. A quadratic fit most accurately characterizes the relationship between IG visibility and fetal stage ($R^2=0.529$, see [Figure 5](#)). The inter-rater variability was very good, with the κ value ranging between 0.623 and 0.709. Each rater repeated the rating after 6 months, and the intra-rater variability showed excellent agreement, with κ value ranging from 0.81 to 0.93. The IG visibility peaks in the second gestational trimester at 25–30 GW, and it is the lowest at the earliest fetal stages and again in the latest fetal trimester ([Figure 5](#)).

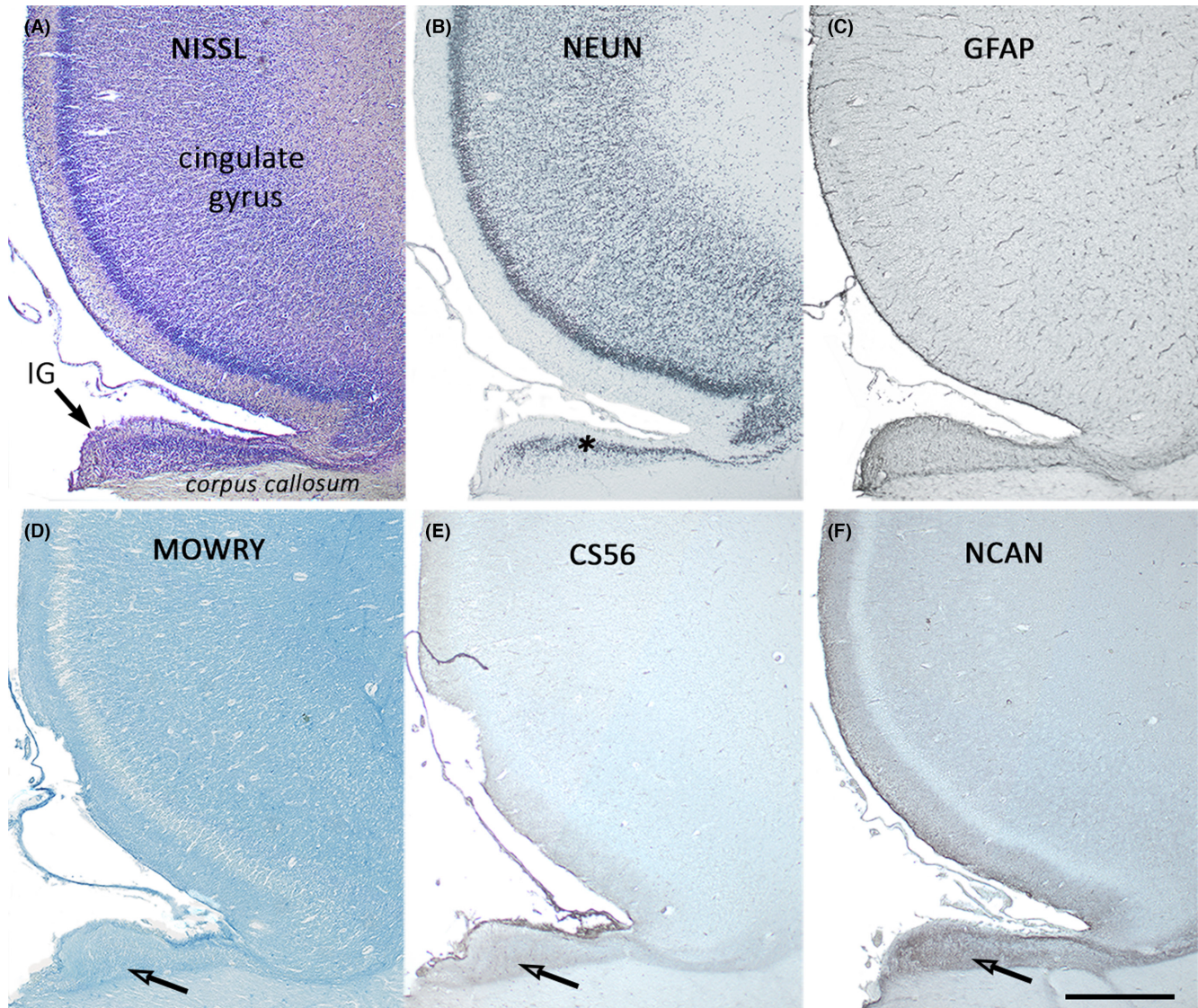


FIGURE 3 The panel presents coronal sections of post-mortem human fetal brain through the ventromedial frontal lobe and the first third of corpus callosum at the stage of 23 GW. Section stained with (A) cresyl violet – modification by Nissl; (D) colloidal iron – modification by Mowry, and by indirect immunohistochemistry for (B) neuronal nuclei protein–NEUN (C), glial fibrillary acidic protein–GFAP, (E) chondroitin sulfate proteoglycans (CS-56), and (F) extracellular neurocan (NCAN). The unilateral presentation of indusium griseum (IG) convexity emerges between the trunk (body) of the corpus callosum (CC) and the juxtapositioned limbus of the most ventral portion of the cingulate gyrus. The glycosaminoglycans-rich CS-56–proteoglycans (E) and neurocan (F) are expressed in an abundant extracellular matrix (empty arrow in D–F). The ECM-rich compartment corresponds to the T2 hyperintensity seen on MR scans (Figure 1E). An asterisk in B marks the IG cortical plate. The magnification scale bar in F represents 500 μ m and refers to all images.

3.3 | Visibility of IG in in vivo MRI

The in vivo 3-T MR imaging (Figure 6A,C) does not provide details and satisfactory resolution enough for IG to be visualized, even in the mid-fetal period when the IG is visible with pmMR. Therefore, we inspected the cases imaged in vivo by 3T MR after the super-resolution of the images were obtained. The two hyperintense spots above the CC were hardly visible in cases at mid-gestation (25+5 GW, Figure 6B,C), which could correspond to the extracellular matrix of the IG.

4 | DISCUSSION

This retrospective observational study deepened our knowledge about the still enigmatic IG roles and functions by understanding the histological substrate of hyperintensity of IG on T2-weighted coronal scans in post-mortem and in vivo 3-T MRI. Furthermore, knowledge of the biological substrate of the MR signal led us to observe the association between IG visibility and the fetal stage (highest during mid-gestation), which allows IG visibility to be considered as a potential imaging biomarker of the regularity of human fetal brain

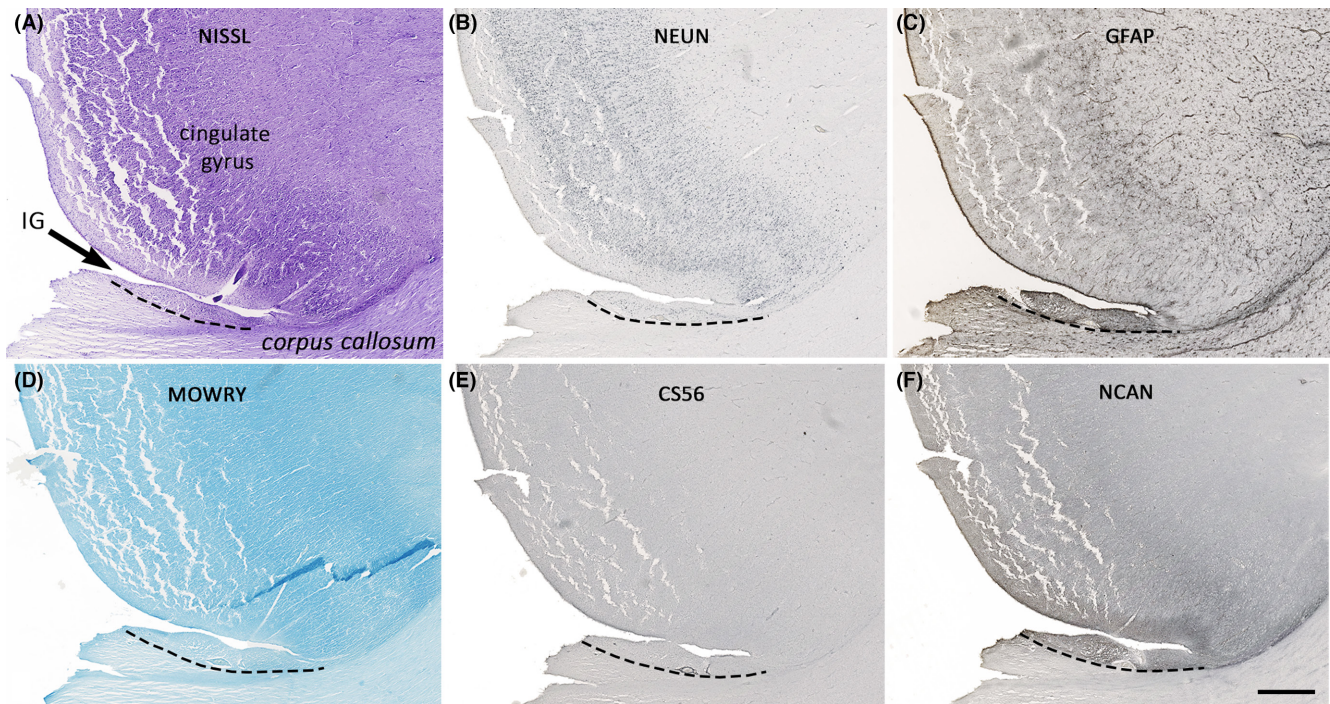


FIGURE 4 The panel presents coronal sections of post-mortem human fetal brain through the ventromedial frontal lobe and the first third of corpus callosum, at the stage of 33 GW, stained with (A) cresyl violet – modification by Nissl; (D) colloidal iron – modification by Mowry, and by indirect immunohistochemistry for (B) neuronal nuclei protein—NEUN (C), glial fibrillary acidic protein—GFAP, (E) chondroitin sulfate proteoglycans (CS-56), and (F) extracellular neurocan (NCAN), showing loss of the abundance of hydrated ECM in transient developmental layers of IG and loss of its convexity in appearance in the coronal plane. The dashed line marks the CC-IG border, which is more challenging to discern at 33GW than 23GW, except for the NCAN immunostaining (F). Note that the size ratio of the IG/cingulate cortex shifts in favor of the cingulate cortex compared to stage 23GW (Figure 2). The scale bar in F marks 500 μ m and refers to all images.

development, more specifically, the regularity of the brain midline development. Although the IG functions during human fetal development, in addition to the morphogenetic roles of the IG' glial cells together with the glial wedge and the callosal septa in corpus callosum genesis,^{18–21} is still unclear, previously shown absence of regression features in IG,³ highly supports its importance and necessity in the human brain. Altogether, this indicates the need to evaluate IG, not only its development and later reorganization at the molecular and histological level, but also to evaluate IG with MR imaging tools, specifically when used in fetal medicine, in assessing the brain midline development.

In our previous study, we showed the histoarchitectonic reorganization of IG during prenatal development into the mature IG and proved the possibility of visualizing fetal IG in pmMR. The current study further elaborates on the significance of IG visibility throughout different fetal stages in the post-mortem, and in vivo fetal MRI. The measures of IG on coronal and sagittal histological sections in different developmental stages are extensively described in Bobić-Rasonja et al.³ After brain fixation and dehydration, which cause shrinkage, the measures of the IG cross-sectional area in histological sections are ca. 5.7–6.7 mm² (measures 0.8–1 mm height in coronal plan) in fetuses at 20–27 GW,³ the period of highest IG-visibility, which explains the size of hyperintense spots on MRI scans of approximately two pixels, depending on the angle of the scanning. However, measuring the

precise IG size or precise ratio between IG and CC thickness in MRI scans is challenging due to the difficulties in determining the border between the ventral IG's and dorsal callosal surface. After the mid-fetal IG visibility peak, two factors decrease the signal intensity toward the last fetal trimester: the loss of hydrated extracellular molecules in the IG and the decrease of the IG cross-sectional area size due to IG reorganization in the medial-lateral and frontal-occipital direction.³ The visibility of IG after 37 GW is similar to that shown in the adult brain.^{12,23}

A recent systematic review of studies on CC morphometry³⁰ has revealed significant heterogeneity in methodology and study design across studies. The referent measures for CC thickness in the mid-sagittal plane on MRI³¹ in adults and neonates are known, which is not the case for fetal CC. According to Rakic and Yakovlev,³² in histological sections (after fixation and dehydration caused shrinkage), the average width of the CC (4 fetuses) age range 18–22 GW was 1.23 mm (genu) and 1.06 mm (body), whereas, at 22–26 GW, CC width was 1.86 mm (genu) and 1.14 mm (body). The average width of the CC (8 fetuses) at 26–30 GW was 2.30 mm (genu) and 1.11 mm (body). However, measured by ultrasound, the mean thickness of the fetal CC at 19 GW is approximately 2 mm (genu) and 1 mm (body), and at 25th GW, 3 mm and 2 mm, respectively.^{33,34} The IG possibly contributes to the measured CC thicknesses in ultrasound imaging morphometry (Figure S1). According to some imaging studies, it should be prudent when the estimated CC thickness is more than

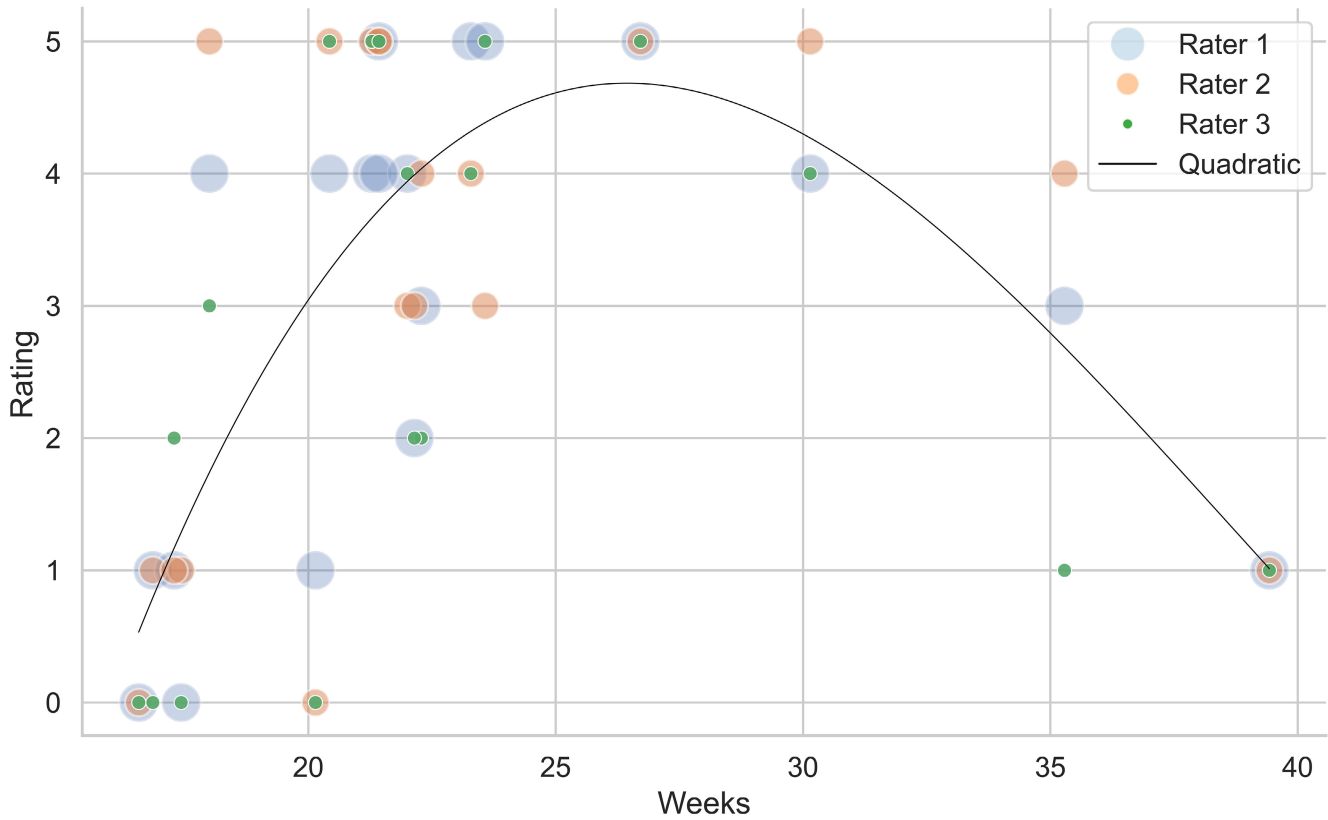


FIGURE 5 The graph shows the association between fetuses' age in gestational weeks and visibility rating score dependent on the agreed IG characteristics (see Material and Methods section). The graph scale ranges from grade 0 to 5 (on the y-axis, IG visibility from 0–5) and gestational weeks from 0 to 40 (on the x-axis). A quadratic fit ($R=0.529$, $p<0.0001$) best describes the association between both.

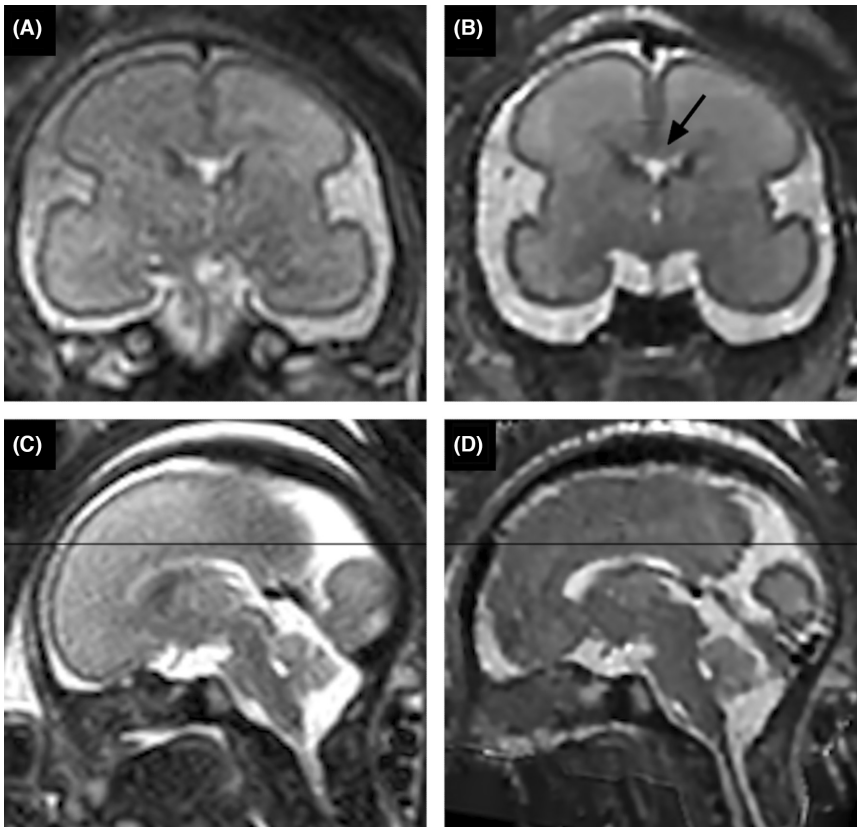


FIGURE 6 Presentation of in vivo 3T MR (T2-w) scans of a human fetal brain at 25+5 GW before (A and C) and after (B and D) super-resolution image processing. Scans in the coronal (A) and sagittal (C) plane of the fetal brain on regular in vivo T2-w 3T MRI reveal no possibility of IG visualization. MR scans after super-resolution processing (B and D) show challenging but potential for visualization of IG as two cloudy spots of higher signal intensity (indicated by a black arrow in B), below the hypointense vertical lines representing the cortical plates of the left and right cingulate regions.

two standard deviations different from the defined mean values since this finding is considered as malformed CC.^{33,35}

Therefore, clinicians need to anticipate that the IG may contribute to the biometrics of CC. Also, other anatomical structures, such as medial and lateral longitudinal Lancisi' striae or aberrant callosal fibers, might interfere with correct measures of the CC.³⁶ Both the anatomical and functional relationship of IG and CC are intertwined in the CC morphogenesis and in CC malgenesis,^{17,18,20,21,37} which contributes to proving that IG visibility in MRI could serve as a bio-imaging reference of normal brain development. Developmental CC disorders are diagnosed around 20 GW or earlier in most clinical cases. Our study shows that the best visibility of the IG is during mid-gestation and is less reliable before and after this period. However, we may expect that the visibility and distinction of IG as well as other small brain structures abundant with ECM, will improve with the advancement of imaging modalities and post-scanning processing resolution progress. A consensus methodology of the highest quality will be essential in defining CC and other malformations and providing appropriate parental counseling.

The main limitation of this study was the number of encompassed cases due to the unavailability of MRI scans without brain pathologies. However, it is comparable to similar studies and has the advantage of in situ imaging, unlike in vitro MRI studies of the fetal brain.³⁸⁻⁴⁰ Future multicentric fetal MR studies, with more cases included, based on the correlation of structural MRI to histology and immunohistochemistry and advances in *in vivo* MRI techniques, could elucidate the role of IG in health and disease as well as its prognostic value. The emerging advanced anatomical and functional imaging technology could be the first step in translating these findings to the *in vivo* setting where the IG serves as an imaging biomarker of the regularity of fetal brain development.

5 | CONCLUSION

The fetal indusium griseum can be visualized on T2-weighted MR images as small, paired, para-medial higher signal intensity areas positioned on the dorsal surface of the corpus callosum (CC) trunk. The visibility of IG is most increased between 25 and 30 GW on pmMRI, which coincides with the transient expression of hydrated ECM in the IG. The IG anatomic position above the callosal trunk could influence the measurements of CC thickness when imaging methods are used at its developmental peak. The progress of the superior resolution imaging modalities may improve the visibility of the IG in *in vivo* MRI soon, strengthening the value of IG as a biomarker in fetal medicine.

AUTHOR CONTRIBUTIONS

Ivana Pogledic, Mihaela Bobić-Rasonja, Christian Mitter, and Natasa Jovanov-Milosevic selected the cases, histological specimens, and MRI scans and performed the formal analysis of IG. Ivana Pogledic, Christian Mitter, and Natasa Jovanov-Milosevic did the IG visibility rating. Ivana Pogledic, Mihaela Bobić-Rasonja, Christian Mitter,

and Andrija Štajduhar prepared the figures. Ernst Schwartz did the super-resolution. Andrija Štajduhar and Pascal A. Baltzer did the formal statistical analyses. Marija Milković-Periša, Maarten Lequin, Gregor Kasprian, and Daniela Prayer participated in the clinical assessment of cases. All coauthors performed literature research, agreed on methodology, participated in the writing, reviewed and edited, read, and approved the final manuscript. Ivana Pogledic and Natasa Jovanov-Milosevic wrote the original draft, Natasa Jovanov-Milosevic did study design and conceptualization. Ernst Schwartz, Miloš Judaš, and Natasa Jovanov-Milosevic acquired funding for the study.

ACKNOWLEDGMENTS

The authors thank Božica Popović and Maja Horvat for excellent technical support in preparing histological specimens and Milos Miljkovic, Martin Steinmetz, and Rebecca Mittermaier for support in MR image acquisition.

FUNDING INFORMATION

The research was financed by the Croatian Science Foundation (IP-2019-04-3182, project acronym BrainECM), the University of Zagreb projects (BM0054; 10 106-22-3116; 10 106-23-2487), Austrian Science Fund (FWF grant I 3925-B27), and the European Union through the European Regional Development Fund (Scientific Center of Excellence for Basic, Clinical and Translational Neuroscience; project GA KK01.1.1.01.0007).

CONFLICT OF INTEREST STATEMENT

The authors have no competing interests to declare.

ETHICS STATEMENT

The MRI part of the study was approved by the Ethics Committee of the Medical School of the University of Vienna (EK 1211/2019) on March 12, 2019 following the Declaration of Helsinki from 2000. The study and the histological and immunohistochemical examinations were approved by the Ethics Committee of the University of Zagreb, School of Medicine, following the Declaration of Helsinki (no.: 380-59-10106-19-111/210 class:641-01/19-02/01) on September 18, 2019.

ORCID

Ivana Pogledic  <https://orcid.org/0000-0001-5465-3005>

Natasa Jovanov-Milosevic  <https://orcid.org/0000-0001-7897-6212>

REFERENCES

1. Di Ieva A, Fathalla H, Cusimano MD, Tschabitscher M. The indusium griseum and the longitudinal striae of the corpus callosum. *Cortex*. 2015;62:34-40.
2. Ren T, Anderson A, Shen WB, et al. Imaging, anatomical, and molecular analysis of callosal formation in the developing human fetal brain. *Anat Rec A Discov Mol Cell Evol Biol*. 2006;288(2):191-204.
3. Bobić Rasonja M, Orešković D, Knezović V, et al. Histological and MRI study of the development of the human Indusium Griseum. *Cereb Cortex*. 2019;29(11):4709-4724.

4. Abbie AA. Cortical lamination in the Monotremata. *J Comp Neurol*. 1940;72(3):429-467.
5. Sturrock RR. Development of the indusium griseum. II. A semithin light microscopic and electron microscopic study. *J Anat*. 1978;125(Pt 3):433-445.
6. Wyss JM, Sripanidkulchai K. The indusium griseum and anterior hippocampal continuation in the rat. *J Comp Neurol*. 1983;219(3):251-272.
7. Ino T, Yasui Y, Itoh K, et al. Direct projections from Ammon's horn to the septum in the cat. *Exp Brain Res*. 1987;68(1):179-188.
8. Kunzle H. The hippocampal continuation (indusium griseum): its connectivity in the hedgehog tenrec and its status within the hippocampal formation of higher vertebrates. *Anat Embryol*. 2004;208(3):183-213.
9. Jinno S, Klausberger T, Marton LF, et al. Neuronal diversity in GABAergic long-range projections from the hippocampus. *J Neurosci*. 2007;27(33):8790-8804.
10. Laplante F, Mnie-Filali O, Sullivan RM. A neuroanatomical and neurochemical study of the indusium griseum and anterior hippocampal continuation: comparison with dentate gyrus. *J Chem Neuroanat*. 2013;50-51:39-47.
11. Kier EL, Fulbright RK, Bronen RA. Limbic lobe embryology and anatomy: dissection and MR of the medial surface of the fetal cerebral hemisphere. *Am J Neuroradiol*. 1995;16(9):1847-1853.
12. Tubbs RS, Prekuc M, Loukas M, Hattab EM, Cohen-Gadol AA. The indusium griseum: anatomic study with potential application to callosotomy. *Neurosurgery*. 2013;73(2):312-315; discussion 316.
13. Sturrock RR. Development of the indusium griseum. I. A quantitative light microscopic study of neurons and glia. *J Anat*. 1978;125(Pt 2):293-298.
14. Sanders M, Petrasch-Parwez E, Habbes HW, Düring MV, Förster E. Postnatal developmental expression profile classifies the Indusium Griseum as a distinct subfield of the hippocampal formation. *Front Cell Dev Biol*. 2021;8:615571.
15. Lippa CF, Smith TW. The indusium griseum in Alzheimer's disease: an immunocytochemical study. *J Neurol Sci*. 1992;111(1):39-45.
16. Fuzik J, Rehman S, Girach F, et al. Brain-wide genetic mapping identifies the indusium griseum as a prenatal target of pharmacologically unrelated psychostimulants. *Proc Natl Acad Sci U S A*. 2019;116(51):25958-25967.
17. Richards LJ, Plachez C, Ren T. Mechanisms regulating the development of the corpus callosum and its agenesis in mouse and human. *Clin Genet*. 2004;66(4):276-289.
18. Jovanov-Milošević N, Benjak V, Kostović I. Transient cellular structures in developing corpus callosum of the human brain. *Coll Antropol*. 2006;30(2):375-381.
19. Jovanov-Milošević N, Čuljat M, Kostović I. Growth of the human corpus callosum: modular and laminar morphogenetic zones. *Front Neuroanat*. 2009;3:6.
20. Jovanov-Milošević N, Petanjek Z, Petrović D, Judaš M, Kostović I. Morphology, molecular phenotypes and distribution of neurons in developing human corpus callosum. *Eur J Neurosci*. 2010;32(9):1423-1432.
21. Čuljat M, Milošević NJ. Callosal septa express guidance cues and are paramedian guideposts for human corpus callosum development. *J Anat*. 2019;235(3):670-686.
22. Paul LK. Developmental malformation of the corpus callosum: a review of typical callosal development and examples of developmental disorders with callosal involvement. *J Neurodev Disord*. 2011;3(1):3-27.
23. Mark LP, Daniels DL, Naidich TP, Borne JA. Limbic system anatomy: an overview. *Am J Neuroradiol*. 1993;14(2):349-352.
24. Nakada T. High-field, high-resolution MR imaging of the human indusium griseum. *Am J Neuroradiol*. 1999;20(3):524-525.
25. Bayer S, Altman J. *The Human Brain During the Second Trimester*. CRC Press, Francis and Taylor Group; 2005.
26. Ebner M, Wang G, Li W, et al. An automated framework for localization, segmentation and super-resolution reconstruction of fetal brain MRI. *NeuroImage*. 2020;206:116324.
27. Jovanov-Milošević N, Judaš M, Aronica E, Kostovic I. Neural ECM in laminar organization and connectivity development in healthy and diseased human brain. *Prog Brain Res*. 2014;214:159-178.
28. Luna LG. Chapter 10: methods for carbohydrates and Mucoproteins. In: Luna LG, ed. *Manual of Histologic Staining Methods of the Armed Forces Institute of Pathology*. 3rd ed. McGraw-Hill Book Company; 1968.
29. Landis JR, Koch GG. The measurement of observer agreement for categorical data. *Biometrics*. 1977;33(1):159-174.
30. Corroenne G, Grevent D, Kasprian G, et al. Corpus callosal reference ranges: systematic review of methodology of biometric chart construction and measurements obtained. *Ultrasound Obstet Gynecol*. 2023;62:175-184.
31. Barkovich AJ, Kjos BO. Normal postnatal development of the corpus callosum as demonstrated by MR imaging. *Am J Neuroradiol*. 1988;9(3):487-491.
32. Rakic P, Yakovlev PI. Development of the corpus callosum and cavum septi in man. *J Comp Neurol*. 1968;132(1):45-72.
33. Malinger G, Zakut H. The corpus callosum: normal fetal development as shown by transvaginal sonography. *AJR Am J Roentgenol*. 1993;161(5):1041-1043.
34. Pashaj S, Merz E, Wellek S. Biometry of the fetal corpus callosum by three-dimensional ultrasound: biometry of the fetal corpus callosum. *Ultrasound Obstet Gynecol*. 2013;42(6):691-698.
35. Lerman-Sagie T, Ben-Sira L, Achiron R, et al. Thick fetal corpus callosum: an ominous sign? *Ultrasound Obstet Gynecol*. 2009;34(1):55-61.
36. Rollins NK. Diffusion imaging of the congenitally thickened corpus callosum. *Am J Neuroradiol*. 2013;34(3):660-665.
37. Schwartz E, Diogo MC, Glatter S, et al. The prenatal morphomechanic impact of agenesis of the corpus callosum on human brain structure and asymmetry. *Cereb Cortex*. 2021;31(9):4024-4037.
38. Wang X, Pettersson DR, Studholme C, Kroenke CD. Characterization of laminar zones in the mid-gestation primate brain with magnetic resonance imaging and histological methods. *Front Neuroanat*. 2015;9:147.
39. Widjaja E, Geibprasert S, Zarei Mahmoodabadi S, Brown NE, Shannon P. Corroboration of normal and abnormal fetal cerebral lamination on post-mortem MR imaging with post-mortem examination. *Am J Neuroradiol*. 2010;31(10):1987-1993.
40. Wang R, Dai G, Takahashi E. High-resolution MRI reveals detailed layer structures in early human fetal stages: in vitro study with histologic correlation. *Front Neuroanat*. 2015;9:150.

SUPPORTING INFORMATION

Additional supporting information can be found online in the Supporting Information section at the end of this article.

How to cite this article: Pogledic I, Bobić-Rasonja M, Mitter C, et al. Fetal *indusium griseum* is a possible biomarker of the regularity of brain midline development in 3T MR imaging: A retrospective observational study. *Acta Obstet Gynecol Scand*. 2024;103:897-906. doi:[10.1111/aogs.14781](https://doi.org/10.1111/aogs.14781)